Acta Crystallographica Section B
Structural Science
ISSN 0108-7681

$Sr_{4+n}Mn^{3+}_4Mn^{4+}_nO_{10+3n}$: a new homologous series of oxygen-vacancy-ordered perovskites built from $Mn^{3+}O_5$ pyramids and $Mn^{4+}O_6$ octahedra

Leopoldo Suescun[a,b]*‡ and Bogdan Dabrowski[b]

[a]Materials Science Division, Argonne National Laboratory, Argonne, IL 60439, USA, and [b]Physics Department, Northern Illinois University, DeKalb, IL 60115, USA

‡ Permanent address: Cryssmat-Lab/DETEMA, Facultad de Química, Universidad de la República, Montevideo, Uruguay, PO Box 1157; leopoldo@fq.edu.uy.

Correspondence e-mail: leopoldo@anl.gov

Received 7 January 2008
Accepted 24 January 2008

A new homologous series of oxygen-vacancy-ordered perovskites with the formula $Sr_{4+n}Mn^{3+}_4Mn^{4+}_nO_{10+3n}$ is proposed based on the structural trends found for the recently described $Sr_4Mn_4O_{10}$, $Sr_5Mn_5O_{13}$ and $Sr_7Mn_7O_{19}$ compounds. These compounds correspond to $n = 0$ ($Sr_4Mn^{3+}_4O_{10}$), $n = 1$ ($Sr_5Mn^{3+}_4Mn^{4+}O_{13}$) and $n = 3$ ($Sr_7Mn^{3+}_4Mn^{4+}_3O_{19}$) members of the series. A linear set of four $Mn^{3+}O_5$ pyramids placed on the *ab* plane and pointing along the $+x$, $-y$, $+y$, $-x$ directions defines the $n = 0$ building block for the series. The nth members can be constructed from blocks containing four pyramids and n $Mn^{4+}O_6$ octahedra with $2/m$ symmetry. Compounds in the related systems $CaMnO_x$ and $LaCuO_x$, containing Mn^{3+} and Cu^{2+} pyramids and Mn^{4+} and Cu^{3+} octahedra have also been found to be members of the series. The size and charge of the *A*-site cation and the apical distortion of the pyramidally coordinated *B*-site cation are shown to be important factors in the stabilization of certain members of the series. A qualitative explanation for the absence of some of the possible members of the series is presented based on these factors.

1. Introduction

Vacancy-ordered oxygen-deficient complex perovskites have been some of the most intensely studied materials ever since the discovery of high-temperature superconductivity in cuprates (Bednorz & Müller, 1986; Wu *et al.*, 1987; Jorgensen *et al.*, 1987, 1990). Since then, over a hundred structures of superconducting compounds have been investigated in detail to determine the structural and physical effect of cation and oxygen-vacancy ordering on superconductivity. This work has led to the observation of common structural features that allowed the identification of several homologous series, and the development of simple building rules that govern systematic formulations of these compounds (Shaked *et al.*, 1994; Yamauchi *et al.*, 1996).

Considering the simple ABO_y perovskites with ordered oxygen vacancies as containing only one type of *A* and *B* cation, a number of publications have already established the common formulations of many series of oxides such as $A_nB_nO_{3n-1}$ (Anderson *et al.*, 1993; Aleksandrov & Beznosikov, 1997; Mitchell, 2002) exemplified by $La_nMn_nO_{3n-1}$ (Abbatista & Borlera, 1981) and $Sr_nFe_nO_{3n-1}$ ($n = 2$, 4, 8 and ∞; Hodges *et al.*, 2000). The $La_nMn_nO_{3n-1}$ homologous series consists of compounds formed by $n-1$ layers of $Mn^{3+}O_6$ octahedra separated by one layer of $Mn^{2+}O_4$ tetrahedra, forming a pattern closely related to the brownmillerite structure $ABO_{2.5}$ (Gallagher *et al.*, 1964) which could be considered as the $n = 2$ member of the series. Although the $La_2Mn_2O_5$ phase has not been isolated so far, the closely related $(La_{0.8}Sr_{0.2})_2Mn_2O_5$

phase has been reported by Casey *et al.* (2006). Abbatista & Borlera (1981) and Borlera & Abbatista (1983) have been able to prepare the $n = 4$ and 8 members of the $La_nMn_nO_{3n-1}$ series. The structural model for $n = 4$, $La_4Mn_4O_{11}$, has been confirmed only recently by Ruiz-González *et al.* (2006). On the other hand, some formulations cannot be considered as true homologous series because they fail to associate structural trends with the cation/anion relations. For example, in $Sr_nFe_nO_{3n-1}$ the $n = 2$ member of the series ($Sr_2Fe_2O_5$) with the brownmillerite structure is formed by $Fe^{3+}O_4$ tetrahedra and $Fe^{3+}O_6$ octahedra, while the $n = 4$ member ($Sr_4Fe_4O_{11}$) contains $Fe^{4+}O_5$ pyramids and $Fe^{3+}O_6$ octahedra. These compounds share a stoichiometric relation, but there is no structural trend associated with them since various coordination types are present for Fe^{3+}. The simple formulation $A_nB_nO_{f(n)}$ [$f(n)$ denotes a function of n] does not explicitly show the existence of different *B*-cation environments in the structure. For the majority of oxygen-vacancy-ordered compounds based on simple perovskites, the *B* cation is found on several crystallographic sites with different coordination geometries and, in general, different formal charges, as observed in $Sr_4Fe_4O_{11}$. For these reasons the use of chemical formulae that express the complexity of the system and the existence of different *B* sites, as well as including structural trends where appropriate, is preferred. A good example of such a formulation is $Ln_{m+n}(Ni^{3+}O_{6/2})_m(Ni^{+}O_{4/2})_n$ (Ln = La^{3+}, Pr^{3+} or Nd^{3+}) proposed by Moriga *et al.* (2002) for $LnNiO_x$ vacancy-ordered compounds formed by layers of octahedrally coordinated Ni^{3+} and square-planar coordinated Ni^{+} stacked along one of the crystallographic directions. The subscript *m* indicates the number of consecutive planes of $Ni^{3+}O_6$ octahedra, while *n* indicates the number of consecutive planes of $Ni^{+}O_4$ squares. To date, the following compounds in this series have been observed: $La_2Ni_2O_5$ ($m/n = 1/1$), $La_3Ni_3O_8$ ($m/n = 2/1$), $Ln_3Ni_3O_7$ ($m/n = 1/2$), $LnNiO_3$ ($m/n = 1/0$; Moriga *et al.*, 2002) and $LaNiO_2$ ($m/n = 0/1$; Hayward *et al.*, 1999). These examples clearly show a rich variety of oxygen-vacancy-ordering schemes observed for simple perovskites and point out the importance of defining homologous series only when structural trends are consistent with chemical formulations.

During research on oxygen-deficient strontium manganites we have found that $Sr_2Mn_2O_5$ (Caignaert *et al.*, 1985) shares several structural features with the recently described compounds $Sr_5Mn_5O_{13}$ and $Sr_7Mn_7O_{19}$ (Suescun *et al.*, 2007). The observed trends suggest that $Sr_2Mn_2O_5$ would be better designated as $Sr_4Mn_4O_{10}$, which conforms to the chemical formulation $Sr_mMn_mO_{3m-2}$ that is also consistent with $Sr_5Mn_5O_{13}$ and $Sr_7Mn_7O_{19}$. In this paper we will examine the structural trends observed for $Sr_4Mn_4O_{10}$, $Sr_5Mn_5O_{13}$ and $Sr_7Mn_7O_{19}$ compounds and propose a set of rules that describe known structures and predict new ones in the $SrMnO_x$ series. We will also generalize the scheme to related systems $CaMnO_x$ and $LaCuO_x$ that show similar oxygen-vacancy arrangements and for which structural similarities have already been noted (Mitchell, 2002; Hadermann *et al.*, 2005). We will also provide arguments for the lack of observation of certain members of the series by considering the geometrical limitations imposed by the *B*-site polyhedral distortions and the *A*-site cation charge and size.

2. $Sr_4Mn_4O_{10}$, $Sr_5Mn_5O_{13}$ and $Sr_7Mn_7O_{19}$: structural trends and building blocks

The compounds $Sr_4Mn_4O_{10}$, $Sr_5Mn_5O_{13}$ and $Sr_7Mn_7O_{19}$ (shown in Figs. 1*a*, *c* and *e*) have been observed in different weight fractions depending on the cooling rate for samples of $SrMnO_x$ fired at $1573 < T < 1673$ K in Ar (Suescun *et al.*, 2007). They can also be prepared without decomposition to SrO and MnO by starting from $SrMnO_3$ in flowing H_2 at 513–573 K. We have used variable-temperature neutron diffraction in 1.2% CO/Ar to investigate the oxygen reduction of the $SrMnO_x$ samples $Sr_7Mn_7O_{19}$, $Sr_5Mn_5O_{13}$ and $Sr_4Mn_4O_{10}$ (Suescun *et al.*, 2008). The $Sr_7Mn_7O_{19}$ phase appears to be stable below 673 K, while $Sr_5Mn_5O_{13}$ converts to $Sr_4Mn_4O_{10}$ above 823 K. $Sr_4Mn_4O_{10}$ decomposes to non-perovskite phases in 1.2% CO/Ar above 873 K. The three compounds oxygenate quickly to oxygen-vacancy-disordered $SrMnO_{3-\delta}$ in the presence of small amounts of O_2 without forming intermediate vacancy-ordered compounds.

2.1. Structural relations among $Sr_4Mn_4O_{10}$, $Sr_5Mn_5O_{13}$ and $Sr_7Mn_7O_{19}$

The main structural similarity among $Sr_4Mn_4O_{10}$, $Sr_5Mn_5O_{13}$ and $Sr_7Mn_7O_{19}$ compounds is their particular linear oxygen-vacancy ordering along one of the cubic perovskite {100} crystallographic directions, leading to the square-based pyramidal and octahedral coordination of Mn cations. Each O^{2-} vacancy in the structure transforms two Mn^{4+} cations into two Mn^{3+} cations that share the vacant site, forming pairs of base-facing square pyramids. The very strong tendency of Mn^{3+} to maintain a square-planar pyramidal coordination favours the localization of the vacant site between the pair of Mn^{3+} pyramids. It has been proposed by Caignaert (1997) that the oxygen-vacancy arrangement in $Sr_4Mn_4O_{10}$ promotes the orbital ordering of Mn^{3+} cations with the half-filled d_{z^2} orbital aligned along the elongated apical direction of the pyramids. This orbital ordering produces a long apical Mn—O bond of ~ 2.05 Å. The apical O atom in one of the pyramids is located at the equatorial position for the nearest pyramid, as shown in Fig. 1(*a*). As a result of this correlation one of the equatorial Mn—O bonds of the nearest pyramid is considerably shorter ~ 1.87 Å, while the three remaining Mn—O bonds have intermediate lengths (1.92–1.96 Å). The same orbital ordering of the Mn^{3+} bonds and the similar Mn—O bond lengths in pyramids have been observed for $Sr_5Mn_5O_{13}$ and $Sr_7Mn_7O_{19}$ compounds (Figs. 1*c* and *e*). Furthermore, for $Sr_7Mn_7O_{19}$ one of the pyramids is connected through its apical oxygen to an octahedron which displays a relatively shorter Mn—O bond (~ 1.80 Å) to accommodate the elongated apical Mn—O bond of the pyramid. Charge ordering has also been proposed for $Sr_5Mn_5O_{13}$ and $Sr_7Mn_7O_{19}$ compounds with Mn^{3+} in pyramidal and Mn^{4+} in octahedral coordination, based on the bond distances and

angles observed (Suescun *et al.*, 2007). This strong tendency of Mn^{3+} towards the formation of elongated pyramids is also observed in non-perovskite compounds with geometrically constrained coordination polyhedra. For example, consider the face-sharing MnO_5 pyramids of the Mn_2O_7 units in $Sr_7Mn_4O_{13}$ (O'Malley *et al.*, 2007) and the Mn_2O_6 units in $Sr_7Mn_4O_{12}$ (Hayward, 2004) for which an apical elongation is observed in $Mn^{3+}O_5$ pyramids that share a face with another elongated $Mn^{3+}O_5$ pyramid, or with a distorted $Mn^{2+}O_4$ tetrahedron.

Regarding the *A* site in the three structures, all Sr^{2+} cations occupy ten-coordinated sites located in the oxygen-vacancy-ordered channels of $Sr_4Mn_4O_{10}$, while some additional 12-coordinated Sr^{2+} cations are found in $Sr_5Mn_5O_{13}$ and $Sr_7Mn_7O_{19}$ outside the channels. The Sr^{2+} cations in the channels are displaced from each other to reduce the unshielded repulsive coulomb interaction among them. This displacement is accompanied by a reduction of the Sr—O bond lengths to compensate for the reduction in number of coordinated anions. In $Sr_4Mn_4O_{10}$ each channel is surrounded by six other channels, two of them parallel but displaced by one perovskite unit in a staircase pattern and four of them perpendicular to it (see Fig. 1*a*). In $Sr_5Mn_5O_{13}$ and $Sr_7Mn_7O_{19}$ the smaller number of vacant sites reduces the number of neighbouring channels, as a result of which only four or two perpendicular channels are found. The pyramidal apical elongation together with a slight rotation of polyhedral units in the *xy* plane, that displaces the O atoms at the end of the channels (linking two pyramids or a pyramid and an octahedron) further from the shifted Sr^{2+} cation, satisfy the required relaxation around the vacant sites.

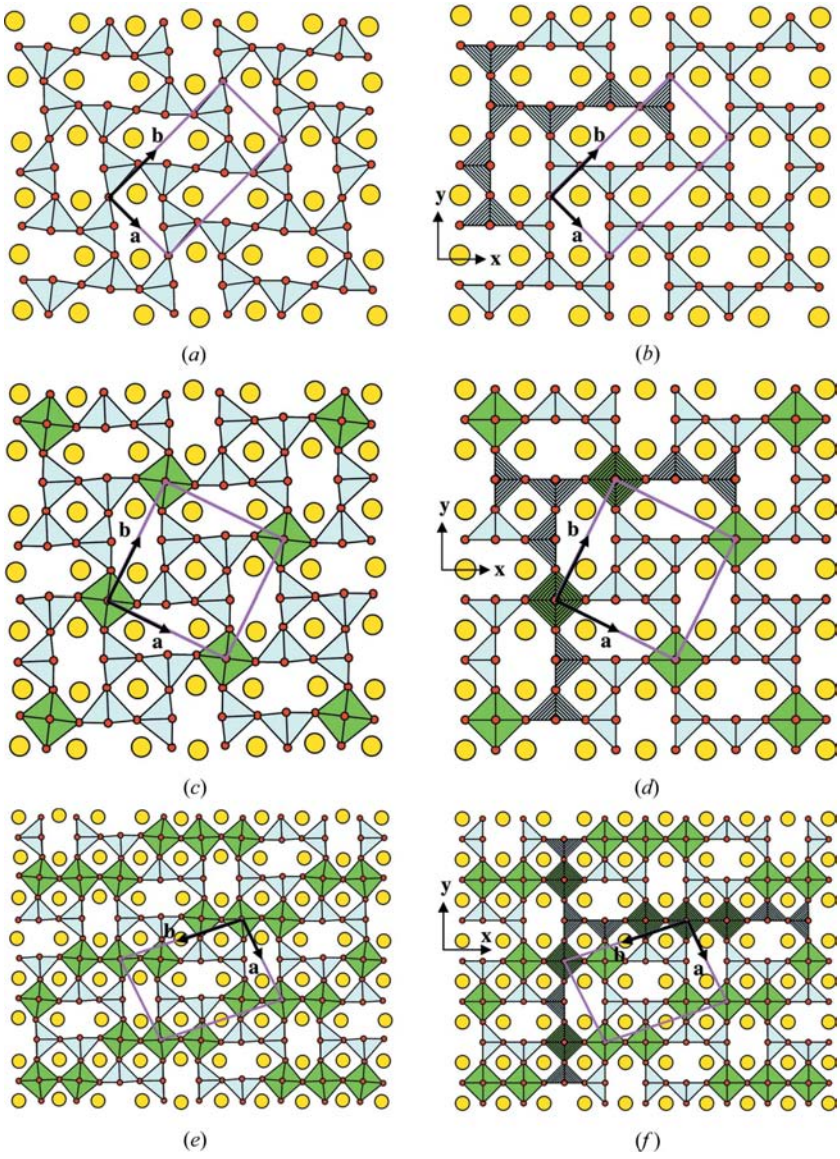

Figure 1
Projections along the *c* axis of structures of (*a*) $Sr_4Mn_4O_{10}$, (*c*) $Sr_5Mn_5O_{13}$ and (*e*) $Sr_7Mn_7O_{19}$ compared with their idealized models (*b*) $A_4B_4O_{10}$, (*d*) $A_5B_5O_{13}$ and (*f*) $A_7B_7O_{19}$. The *x* and *y* axes indicate *a* and *b* lattice directions in the original cubic perovskite. The orientation of the unit cell was selected to allow a direct comparison of building blocks, therefore, the crystallographic *c* axis in (*e*) and (*f*) points downwards.

These distortions are easily observed by comparing the real $Sr_4Mn_4O_{10}$, $Sr_5Mn_5O_{13}$ and $Sr_7Mn_7O_{19}$ structures (Figs. 1*a*, *c* and *e*) with the idealized $A_4B_4O_{10}$, $A_5B_5O_{13}$ and $A_7B_7O_{19}$ models (shown in Figs. 1*b*, *d* and *f*), which are obtained by removing lines of O atoms along the [001] direction from the regular cubic perovskite ABO_3 network. The synergic combination of three factors, orbital ordering of Mn^{3+} cations, charge ordering of Mn^{3+}/Mn^{4+} and relaxation of the coulomb interaction around the vacant sites, are considered to be the three main physical factors responsible for the stabilization of $Sr_5Mn_5O_{13}$ and $Sr_7Mn_7O_{19}$ structures, with respect to the possible vacancy-disordered ones. It will be discussed later that elimination of one or more of these three stabilization factors could explain the lack of observation of certain members of the $Sr_mMn_mO_{3m-2}$ series.

2.2. Building blocks for $Sr_4Mn_4O_{10}$ and $Sr_5Mn_5O_{13}$

In an attempt to rationalize the systematic structural observations in $Sr_4Mn_4O_{10}$, $Sr_5Mn_5O_{13}$ and $Sr_7Mn_7O_{19}$ a set of rules is proposed to build their structures. The development of the rules will start with structures of $Sr_4Mn_4O_{10}$ and $Sr_5Mn_5O_{13}$, and then will be applied to the $Sr_7Mn_7O_{19}$ compound.

In $Sr_4Mn_4O_{10}$ the vacancy-ordering pattern defines linear groups of four pyramids pointing consecutively from left to right along $+x$, $-y$, $+y$ and $-x$ (with respect to the cubic perovskite axes), as highlighted in Fig. 1(*b*). Groups of four pyramids are terminated

Table 1
Idealized compounds in the $A_{4+n}B_{4+n}O_{10+3n}$ series, as obtained from the proposed building blocks.

Examples of observed compounds and their space groups are given in the last two columns of the table. The global oxygen content x for the formulation ABO_x is obtained as $x = 3 - 2/(4 + n)$. The unit-cell dimensions given are based on the simple cubic perovskite with $a = a_P$

n	x in ABO_x	Pyramid/octahedra	Cell parameters† (a, b, c, γ, V)	Space group (ideal)†	Observed	Space group†
0	2.5	pppp	$2^{1/2}a_P$ $2(2)^{1/2}a_P$ a_P $4V_P$	*Pbam* (55)	Sr/Ca–Mn	*Pbam*
					Sr/La/Nd–Cu	*Pbam*
1	2.6	ppopp	$5^{1/2}a_P$ $5^{1/2}a_P$ a_P $5V_P$	*P*4/*m* (83)	Sr–Mn	*P*4/*m*
					La/Nd–Cu	*P*2/*m*
2	2.667	ppoopp	$2a_P$ $10^{1/2}a_P$ a_P $\gamma = 108.4$ $6V_P$	*P*2/*m* (10)	–	–
		poppop	$2^{1/2}a_P$ $3(2)^{1/2}a_P$ a_P $6V_P$	*Pbmm* (*Pmma*, 51)	Ca–Mn	N.a.
3	2.714‡	ppooopp/popopop	$5^{1/2}a_P$ $10^{1/2}a_P$ a_P $\gamma = 98.2$ $7V_P$	*P*2/*m* (10)	Sr–Mn	*P*2/*m*
4	2.75	ppoooopp/popoopop	$2(2)^{1/2}a_P$ $10^{1/2}a_P$ a_P $\gamma = 116.6$ $8V_P$	*P*2/*m* (10)	–	–
		pooppoop	$2^{1/2}a_P$ $4(2)^{1/2}a_P$ a_P $8V_P$	*Pbam* (55)	Ca–Mn	N.a.

† For monoclinic unit cells c was taken as the unique axis. ‡ The oxygen content of this phase corresponds to the rational number 7/19 = 2.714285.

at vacant sites, leaving the end pyramids pointing inwards and having one vacancy on each side. In $Sr_5Mn_5O_{13}$, a similar linear group is formed by two pyramids pointing along $+x$, $-y$ (one octahedron) and two other pyramids pointing along $+y$ and $-x$, ($+x$, $-y$, o, $+y$, $-x$), as shown in Fig. 1(*d*). Again the groups terminate at vacant sites with the end pyramids pointing inwards and have one vacant site on each side. In both cases these groups of polyhedra can be used to reconstruct the plane and the complete three-dimensional structure by matching vacant sites at both sides and ends of the blocks, and using translations along the fundamental lattice vectors or linear combinations of them, as shown in Figs. 1(*b*) and (*d*). Given the vacancy-ordering arrangement, a group of four pyramids, or four pyramids and one octahedron, is formed in both the x and y directions in $Sr_4Mn_4O_{10}$ and $Sr_5Mn_5O_{13}$. Conversely, given the group of polyhedra, only one vacancy-ordering arrangement can be constructed starting with the group in the x or y direction. The space-group symmetry of both $Sr_4Mn_4O_{10}$ and $Sr_5Mn_5O_{13}$ structures (*Pbam* and *P*4/*m* space groups) allows polyhedral groups in the x or y directions to be related by symmetry, as can be observed in Fig. 1.

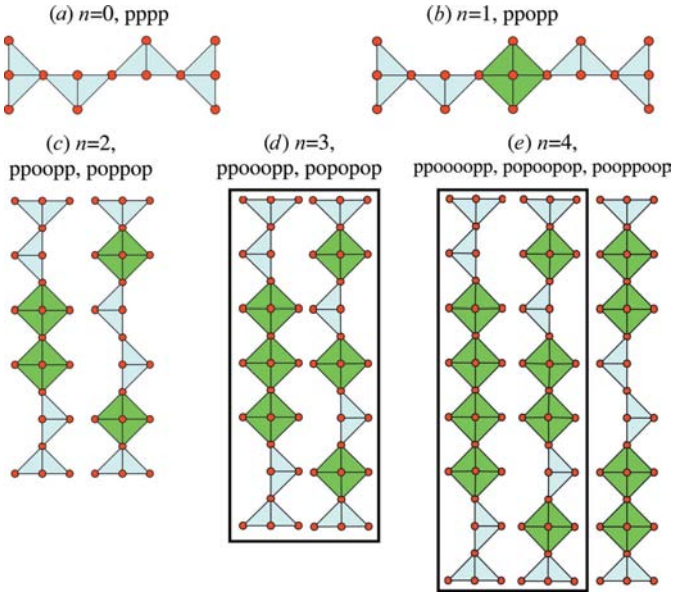

Figure 2
Building blocks of the $Sr_{4+n}Mn_4^{3+}Mn_n^{4+}O_{10+3n}$ series of compounds (*a*) n = 0 or pppp, (*b*) n = 1 or ppopp, (*c*) n = 2 in two variants ppoopp and poppop, (*d*) n = 3 in two variants ppooopp and popopop, and (*e*) n = 4 in three variants ppoooopp, popoopop and pooppoop. The blocks in boxes combine in one structural arrangement.

Fig. 2 shows isolated building blocks formed by four pyramids (pppp in Fig. 2*a*), and four pyramids and one octahedron (ppopp, Fig. 2*b*). The presence of common 2/*m* symmetry in $Sr_4Mn_4O_{10}$ and $Sr_5Mn_5O_{13}$ structures (*Pbam* and *P*4/*m* space groups have both twofold axes parallel to, and mirror planes perpendicular to, *c*) means that both pppp and ppopp blocks also display 2/*m* symmetry. Starting with the symmetrical pppp building bock, the ppopp block is obtained by the addition of one octahedron in the centre of the block keeping its 2/*m* symmetry. As such, these groups allow for structural distortions to accommodate charge and orbital order which is observed experimentally through an increase in the apical Mn—O bond distances and a decrease in the corresponding equatorial bonds, and rotation of the polyhedra. Therefore, the idealized pppp and ppopp groups can be transformed into observed ones with accurate bond distances and angles. Table 1 shows the structural details of the idealized atomic arrangements generated from the blocks corresponding to $A_4B_4O_{10}$ and $A_5B_5O_{13}$ models of Figs. 1(*b*) and (*d*).

The number of octahedra in the blocks (n) generates different members of the homologous series $Sr_{4+n}Mn_{4+n}O_{10+3n}$, where n = 0 for the pppp block containing no octahedra and n = 1 for the ppopp block. The $n > 1$ building blocks could be obtained by adding more octahedra to the linear pppp group. As is the case of the ppopp block, this will be achieved by preserving the 2/*m* symmetry, provided that the geometrical relations among vacant sites such as relative orientation and number of neighbours are fulfilled. As the number of added octahedra increases, the internal structure of the group becomes more complex. Several different building

blocks are constructed for the same n (see Fig. 2), while preserving the 2/m symmetry leads in some cases to dissimilar structural patterns, as will be discussed in the following sections.

2.3. Extension of building-blocks description to $Sr_7Mn_7O_{19}$

The compound $Sr_7Mn_7O_{19}$ (Fig. 1*e*) is also a unique member of the $Sr_{4+n}Mn_{4+n}O_{10+3n}$ series and its structure could be explained using the building-block description introduced in the previous section. Let us start by observing that it contains three octahedra per unit cell, therefore, it is the $n = 3$ member of the series.

Two ways to arrange three octahedra in the pppp block while retaining the 2/m symmetry and keeping pyramids at both ends of the block can be devised: ppooopp and popopop, as shown in Fig. 2(*d*). This is different from the $n = 0$ and $n = 1$ compounds, where only one block was possible. However, as will be shown in the following for the $n = 3$ case, the two building blocks are not independent as they generate each other when a complete $Sr_7Mn_7O_{19}$ structural arrangement is constructed.

Starting with the horizontal ppooopp block, the entire pattern corresponding to the idealized $A_7B_7O_{19}$ arrangement (Fig. 1*f*) is built by the application of a linear combination of the translation vectors **a** and **b**. In an analogous manner, using a vertical popopop block, the ppooopp pattern corresponding to the idealized $A_7B_7O_{19}$ arrangement is built. As a result, the popopop block forms in an orthogonal direction to the ppooopp block, and *vice versa*, once the structure is built using one of them. Therefore, both ppooopp and popopop blocks (highlighted in Fig. 1*f*) lead to a unique structural arrangement observed for the $Sr_7Mn_7O_{19}$ compound. The $P2/m$ space group of $Sr_7Mn_7O_{19}$ provides no symmetry relation between the x and y directions of the original perovskite structure, eliminating the need for identical ordering of polyhedra in both directions. However, the inherent 2/m symmetry of the structure is again preserved for the building blocks in both the x and y directions, which are no longer equivalent. It will be immediately shown that this is not the general case when multiple possible building blocks exist.

The proposed building-block numbering scheme is useful to formulate the compounds belonging to this homologous series by showing the full complexity of the system. For each member of the series n defines the number of octahedrally coordinated Mn^{4+} cations, while the number of $Mn^{3+}O_5$ pyramids is 4. The chemical formula for the series should then read $Sr_{4+n}Mn_4^{3+}Mn_n^{4+}O_{10+3n}$. With this formulation $Sr_4Mn_4O_{10}$ ($Sr_4Mn_4^{3+}O_{10}$), $Sr_5Mn_5O_{13}$ (or $Sr_5Mn_4^{3+}Mn^{4+}O_{13}$) and $Sr_7Mn_7O_{19}$ (or $Sr_7Mn_4^{3+}Mn_3^{4+}O_{19}$) are the $n = 0$, 1 and 3 members of the series.

3. Oxygen ordered phases with non-unique framework connectivity

The proposed building-block description will now be used to construct the idealized structures of the other compounds in the series. These structures are considered together due to their special characteristic, the non-unique frameworks generated from specific building blocks. We will reason that the lack of observation of the corresponding compounds may be due, among particular features of each pattern, to the degeneracy of structural patterns for a specific oxygen content leading to frustration and the absence of long-range order. Fig. 3 and Table 1 show two dissimilar structures for $n = 2$ ($Sr_6Mn_6O_{16}$) and $n = 4$ ($Sr_8Mn_8O_{22}$) members of the series, that have not been observed so far for the $SrMnO_x$ system.

3.1. $n = 2$, $Sr_6Mn_6O_{16}$

The addition of two octahedra to the four pyramids pppp, while retaining 2/m symmetry and keeping pyramids at both ends, could be performed in two ways, ppoopp or poppop, as shown in Fig. 2(*c*). By matching vacancies in successive blocks to reconstruct the xy plane of the hypothetical compound $Sr_6Mn_6O_{16}$, two structures are built: ppoopp-$A_6B_6O_{16}$ and poppop-$A_6B_6O_{16}$, as shown in Figs. 3(*a*) and (*b*), with the resulting lattice translation vectors shown. Table 1 shows the expected unit-cell parameters and space groups of these model structures.

We will argue now that in addition to the structural degeneracy, several structural features for both $A_6B_6O_{16}$ arrangements make them less likely to be observed experimentally than $Sr_{4+n}Mn_4^{3+}Mn_n^{4+}O_{10+3n}$ ($n = 0$, 1 and 3). In ppoopp-$A_6B_6O_{16}$ the alternation of vacancies along the crystallographic b-axis direction coincides with the observed alternation along (110) in $Sr_4Mn_4O_{10}$ and $Sr_5Mn_5O_{13}$, and (010) in $Sr_7Mn_7O_{19}$ (see Figs. 1*b*, *d* and *f*). This makes the ppoopp-$A_6B_6O_{16}$ model a clear member of the homologous series. However, the connectivity of polyhedra is such that two out of four pyramids would be linked by the apical oxygen. Additionally, channels formed by vacant sites are aligned along the original perovskite y direction (or crystallographic a direction), unlike in the $n = 0$, 1 and 3 members of the series. These two features violate the cooperative distortions described previously and would reduce the structural stability of this pattern, if formed in a real structure, owing to the large ion displacements expected to occur, as observed for $n = 0$, 1 and 3 compounds. Additionally, the building block does not reproduce itself in both directions, generating an infinite chain of pyramids and octahedra along the perovskite y axis that alternates in the x direction with apex-linked pyramids separated by vacant sites when a building block in the x direction is used to build the pattern. This produces an additional destabilizing feature owing to the large anisotropy of the x and y directions. In poppop-$A_6B_6O_{16}$ the relative orientation of the vacancies differs markedly from those observed in $n = 1$, 2 (ppoopp) and 3, resembling that observed in the a-axis direction for $n = 0$ (see Fig. 1*b*). Indeed, the pattern for poppop-$A_6B_6O_{16}$ can be built by shifting layers of vacancies along the a-axis direction in $A_4B_4O_{10}$ by one perovskite unit in the y direction and filling the space generated with a layer of octahedra. Each octahedron is connected to two neighbouring pyramids through their apical oxygen. The same two O atoms are located at the end of mutually perpendicular channels.

These two features again seem to destabilize the structure through uncorrelated ion displacements, because each octahedron would have two short Mn—O bonds that would form an angle smaller than 90° to shift oxygen ions away from the Sr^{2+} cations that are displaced by unshielded electrostatic repulsion within the channels.

These destabilizing structural features in addition to the degeneracy of the network arrangements are probably responsible for the lack of observation of compounds with the composition $SrMnO_{16/6\,=\,2.667}$. In addition, a sample with the overall composition $SrMnO_{2.668}$ has turned out to be a mixture of $Sr_5Mn_5O_{13}$ and $Sr_7Mn_7O_{19}$ phases (Suescun *et al.*, 2007; 2008), proving the instability of the structural arrangements made from the symmetric ppoopp and poppop, and also other asymmetric pooppp and popopp building blocks (not included in our description). Therefore, the predictions of the proposed building-block scheme are consistent with the observed phases $Sr_{4+n}Mn_{4+n}O_{10+3n}$ for n = 0–3.

3.2. n = 4, $Sr_8Mn_8O_{22}$

The addition of four octahedra to the four pyramids yields three blocks which satisfy 2/*m* symmetry: ppooooopp, popoopop and poopppoop, as shown in Fig. 2(*e*). These blocks can be used to construct a plane of the hypothetical compound $Sr_8Mn_8O_{22}$, yielding the two structural patterns shown in Figs. 3(*c*) and (*d*). Unit-cell dimensions and the symmetry of these patterns are listed in Table 1. The building blocks ppooooopp and popoopop (Fig. 3*c*) combine together in one single arrangement, as was observed for ppooopp and popopop blocks for n = 3. The poopppoop block forms an arrangement that reproduces itself in both orthogonal directions of the plane (Fig. 3*d*). As a result, two dissimilar structural arrangements are built based on four pyramids and four octahedral building blocks. The relative orientation of channels formed around vacant sites for ppooooopp/popoopop-$A_8B_8O_{22}$ resemble the patterns observed for n = 1, 2 (ppoopp) and 3. The pattern for poopppoop-$A_8B_8O_{22}$ can be built by adding two rows of octahedra between neighbouring vacancy lines along the *a* axis in $A_4B_4O_{10}$, or adding one extra row of octahedra next to the existing one in poppop-$A_6B_6O_{16}$. Both observations confirm, once again, the very similar geometrical features shared by all members of the proposed homologous series.

None of the two possible arrangements for n = 4 displays any of the destabilizing structural features observed for n = 2 models that would prevent their experimental observation. The ppooopp/popoopop-$A_8B_8O_{22}$ arrangement resembles the $Sr_7Mn_7O_{19}$ structure in the relative orientation of polyhedra around the vacant sites and the relative positioning of the channels. The poopppoop-$A_8B_8O_{22}$ model resembles that of poppop-$A_6B_6O_{16}$, however, the existence of two layers of octahedra separating the channels (instead of one in poppop-$A_6B_6O_{16}$) creates only one short bond for octahedra connected to an apical oxygen from the neighbouring pyramid. Since none of the destabilizing features are present for $Sr_8Mn_8O_{22}$ arrangements, corresponding to a composition $SrMnO_{2.75}$, a reason for the lack of observation of phases with this comparison may be the coexistence of both orders in small domains, leading to frustration of long-range ordering and the observation of a disordered average structure. This seems to be the case for the closely related $CaMnO_x$ system (see §4).

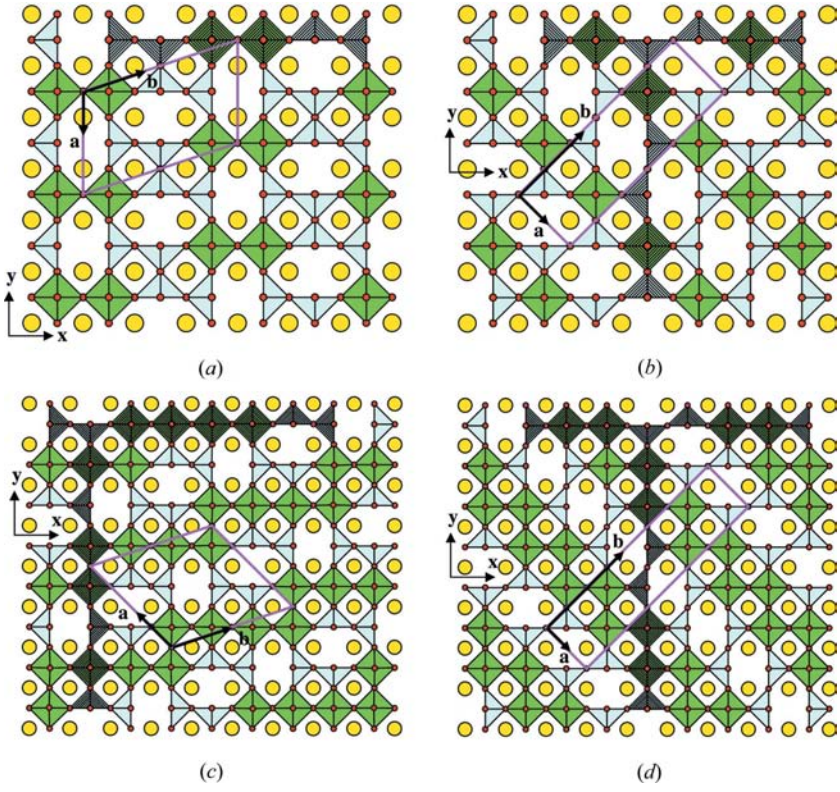

Figure 3
Hypothetical structures of the formula $A_6B_6O_{16}$ and $A_8B_8O_{22}$ formed with n = 2 blocks (*a*) ppoopp and (*b*) poppop, and n = 4 blocks (*c*) ppooooopp/popoopop and (*d*) pooppoop. The orientation of the unit cell was selected to allow a direct comparison of building blocks, therefore, the crystallographic *c* axis in (*c*) points downwards.

3.3. N > 4 members of $Sr_{4+n}Mn_4^{3+}Mn_n^{4+}O_{10+3n}$ and the asymmetric building blocks

The extension of the building-block scheme to n > 4 leads to results which are similar to n = 2 and 4. In all the cases inspected (n = 5, 6, 7 and 8) three or more different blocks produce two or more structural arrangements that show a polyhedral connectivity that reproduces features of n = 2, 3 or 4 compounds. To the best of our knowledge, no oxygen-vacancy-ordered structure has been observed with the structural patterns derived from blocks with n >

4. For these lower-vacancy concentration compounds with $x \geq 2.75$ disordered phases have been reported (Suescun *et al.*, 2008).

The elimination of the 2/*m* symmetry condition would lead to a large number of new structural patterns causing increased degeneracy and frustration, as well as generating patterns showing, in many cases, destabilizing features such as those described for $n = 2$ models. For $n = 1$ and $n = 3$ members of the series, this source of frustration has not been observed, therefore structures derived from asymmetric building blocks seem not to be viable when compared with those derived from symmetric building blocks. In addition, since no structures consistent with these asymmetric building blocks have been reported for any value of *n*, we will not discuss them here. A complete derivation of different possible structures with different types of asymmetric building blocks will be published separately.

4. Oxygen-vacancy-ordered phases with $A_{4+n}B_{4+n}O_{10+3n}$ structure types

In an attempt to generalize our results to other oxygen-deficient vacancy-ordered perovskites, a search for simple perovskites with structures consistent with the $Sr_{4+n}Mn_4^{3+}Mn_n^{4+}O_{10+3n}$ series was performed. The cuprates and manganates described below have been found to comply with our structural rules. The discussion that follows only focuses on simple perovskites, however, several *A* or *B* site-doped perovskites have also been found to display structures consistent with our formulation.

4.1. The $CaMnO_x$ system

The compound $CaMnO_3$ has been reported to form a large number of oxygen-deficient phases $CaMnO_x$, with $2.5 < x < 3$ (Reller *et al.*, 1982). $Ca_2Mn_2O_5$ (or $Ca_4Mn_4O_{10}$) was the first reported vacancy-ordered perovskite manganate containing Mn^{3+} pyramids (Poeppelmeier *et al.*, 1982). This phase is also the only oxygen-vacancy-ordered phase in the $CaMnO_x$ system that has been fully characterized in bulk samples by diffraction techniques. Applying high-resolution transmission electron microscopy and electron diffraction to $CaMnO_{2.667}$, Reller *et al.* (1984) found a phase with the unit-cell dimensions

$$a = 2^{1/2}a_P, \quad b = 3(2)^{1/2}a_P, \quad c = a_P, \tag{1}$$

and for $CaMnO_{2.75}$ another one with

$$a = 2^{1/2}a_P, \quad b = 4(2)^{1/2}a_P, \quad c = 2a_P. \tag{2}$$

These two observed unit cells correspond (in the direction normal to the vacancy lines) to the compounds proposed here in the $Sr_{4+n}Mn_4^{3+}Mn_n^{4+}O_{10+3n}$ series for $n = 2$ poppop and $n = 4$ pooppoop listed in Table 1 and shown in Figs. 3(*b*) and (*d*), respectively. For each of the compounds the authors proposed more than one vacancy-ordering arrangement consistent with unit-cell dimensions, but found insufficient experimental evidence to decide which one represented the actual structure. None of their structural models proposed for $CaMnO_{2.667}$ correspond to patterns derived from our building block description. On the other hand, one of the structures proposed for $CaMnO_{2.75}$ is identical to the $n = 4$ pooppoop-$A_8B_8O_{22}$ pattern shown in Fig. 3(*d*). Pyramidal/octahedral tilting (like that observed in $CaMnO_3$) and vacancy displacement in consecutive layers were used as possible explanations for the doubling of the *c* axis. Chiang & Poeppelmeier (1991) applied neutron powder diffraction to study a sample with the composition $CaMnO_{2.75}$. They again found the unit cell

$$a = 2^{1/2}a_P, \quad b = 4(2)^{1/2}a_P, \quad c = 2a_P, \tag{3}$$

consistent with our pooppoop-$A_8B_8O_{22}$ model (except for doubling of the *c* axis), and tested several vacancy-ordering arrangements consistent with the observed unit cell, however, none of them gave satisfactory fit to the data.

4.2. The $ACuO_x$ system (*A* = La, Nd, Sr)

Several oxygen-deficient cuprates have been described that display complex oxygen-vacancy-ordering arrangements. Among them $BaLa_4Cu_5O_{13}$ (tetragonal, *P*4/*m*) was the first oxygen-deficient compound showing the ppopp-$A_5B_5O_{13}$ vacancy ordering in addition to Ba/La cation ordering (Michel *et al.*, 1985). The $La_5Cu_5O_{13}$ (Bringley *et al.*, 1990) and $Nd_5Cu_5O_{13}$ (Chen *et al.*, 1995) compounds have been described using the same vacancy-ordering arrangements. However, both compounds show a monoclinic unit cell in the *P*2/*m* space group obtained by elimination of the fourfold axis present in the ideal $A_5B_5O_{13}$ (tetragonal *P*4/*m* structure shown in Table 1), but keeping the 2/*m* symmetry found in related compounds, yielding a cell with $a \simeq b$ and $\gamma \simeq 90^\circ$ (unique *c* axis). These two compounds could be regarded as the $n = 1$ members of the $A_{n+4}Cu_{n+4}O_{10+3n}$ series. Additionally, the compounds $La_2Cu_2O_5$ (or $La_4Cu_4O_{10}$; Bringley *et al.*, 1990), $Nd_2Cu_2O_5$ (or $Nd_4Cu_4O_{10}$; Chen *et al.*, 1995) and $Sr_2Cu_2O_5$ (or $Sr_4Cu_4O_{10}$; Chen *et al.*, 1996) have also been described and could be considered as the $n = 0$ members of the series.

It is interesting to note that the $n = 0$ and $n = 1$ cuprates containing *A* = La/Nd are similar to the $n = 0$ and $n = 1$, *A* = Sr, manganates, not only from a structural point of view but also from an electronic one. For $La_5Cu_5O_{13}$ ($n = 1$), Cu is found in pyramidal and octahedral coordination, and the average Cu valence is 2.2+. La Placa *et al.* (1995) have proposed a charge-ordering model in this compound with four Cu^{2+} occupying pyramids and one Cu^{3+}-occupying octahedra giving an average charge of $(4Cu^{2+} + 1Cu^{3+})/5 = Cu^{2.2+}$. A similar charge-ordering pattern of Mn^{3+} in pyramids and Mn^{4+} in octahedra has been described for $Sr_5Mn_5O_{13}$ (Suescun *et al.*, 2007). Therefore, the $La_{4+n}Cu_4^{2+}Cu_n^{3+}O_{10+3n}$ formulation applies to $La_2Cu_2O_5$ and $La_5Cu_5O_{13}$ compounds. The coincidence of structural patterns can be extrapolated even further by considering the similar chemical behaviour of transition metals with d^n and d^{n+5} electronic configurations; Mn^{3+} is a d^4 cation, while Cu^{2+} displays a d^9 electronic configuration. At the same time, Mn^{4+} is a d^3 cation, while Cu^{3+} is d^8. Both Mn^{3+} and Cu^{2+} atoms display a noticeable Jahn–Teller effect in an octahedral coordination and a marked tendency towards

Table 2
$A-A$ distances (Å) in the observed $A_4B_4O_{10}$, $A_5B_5O_{13}$ and $A_7B_7O_{19}$ compounds.

$\langle A-A\rangle_{xy}$ is the average distance among A cations in the channels. $\langle A-A\rangle_z$: the average $A-A$ distance in two consecutive 001 planes (equals the c-axis length). Percentage variation E (%) of $\langle A-A\rangle_{xy}$ with respect to $\langle A-A\rangle_z$ in each compound are given as a measure of the deformation of the network.

Compound	Space group	$\langle A-A\rangle_{xy}$	$\langle A-A\rangle_z$	E (%)	Reference
$n = 0$					
$Ca_4Mn_4O_{10}$	*Pbam*	4.314	3.735	15.5	Poeppelmeier *et al.* (1982)
$Sr_4Mn_4O_{10}$	*Pbam*	4.309	3.807	13.2	Suescun *et al.* (2007)
$Sr_4Cu_4O_{10}$	*Pbam*	4.170	3.731	11.8	Chen *et al.* (1996)
$La_4Cu_4O_{10}$	*Pbam*	4.526	3.880	16.6	La Placa *et al.* (1993)
$La_4Cu_4O_{10}$	*Pbam*	4.520	3.880	16.5	Khasanova *et al.* (1996)
$La_4Cu_4O_{10}$	*Pbam*	4.535	3.880	16.9	Hiroi (1996)
$Nd_4Cu_4O_{10}$	*Pbam*	4.664	3.806	22.5	Chen *et al.* (1995)
$n = 1$					
$Sr_5Mn_5O_{13}$	*P4/m*	4.228	3.810	11.0	Suescun *et al.* (2007)
$La_5Cu_5O_{13}$	*P2/m*	4.556	3.831	18.9	la Placa *et al.* (1995)
$Nd_5Cu_5O_{13}$	*P2/m*	4.588	3.777	21.5	Chen *et al.* (1995)
$n = 3$					
$Sr_7Mn_7O_{19}$	*P2/m*	4.151	3.808	9.0	Suescun *et al.* (2007)

pyramidal coordination to facilitate, through orbital ordering, minimization of the interaction energy of the unpaired e_g electron with the O^{2-} ions. Mn^{4+}, on the other hand, displays empty e_g orbitals, while Cu^{3+} usually displays a high-spin configuration state with both e_g electrons unpaired. Neither of these cations shows significant Jahn–Teller distortion in an octahedral environment, leading to approximately regular BO_6 octahedra as observed in $Sr_5Mn_5O_{13}$, $Sr_7Mn_7O_{19}$, $Nd_5Cu_5O_{13}$ and $La_5Cu_5O_{13}$.

5. *A*-site size and charge effect and structural building blocks

In §2.3 the geometrical relations among pyramids and octahedra in $Sr_6Mn_6O_{16}$ were used to explain the lack of observation of the $n = 2$ structural arrangements. In general, consideration of only the $B-O$ framework may not be enough to predict if a proposed phase is expected to be observed or not. The influence of the size and charge of the A cation will be discussed here in order to give a qualitative explanation for the lack of observation of some possible structures for the $CaMnO_x$ and La/$NdCuO_x$ compounds.

5.1. Size effect

Table 2 shows the observed average near-neighbour $A-A$ distances for all the reported compounds of the $AMnO_x$ and $ACuO_x$ series. $\langle A-A\rangle_{xy}$ represents the average distance between two A cations in a channel in the xy plane and $\langle A-A\rangle_z$ represents the average distance of the A cations in successive planes or along z (the c-axis direction in all cases). The c-axis distance is taken to be a reference for the $A-A$ separation, typical for a fully oxygenated cubic perovskite, and the elongation of the $A-A$ distance in the channels is calculated with respect to $\langle A-A\rangle_z$ and expressed as a percentage in E (%). The comparison among manganites and cuprates is facilitated by the similarity of ionic radii of high-spin Mn^{3+} and Cu^{2+} (0.645 and 0.65 Å; Shannon, 1976) that allows the observed differences to be solely ascribed to changes in the ionic radii of A, excluding the $Sr_4Cu_4O_{10}$ compound where a significantly smaller Cu^{3+} cation is present (ionic radii 0.54 Å corresponding to coordination number 6). Additionally, the average $\langle A-A\rangle_z$ separation in all the compounds can be directly correlated to the size of the A cation: Ca^{2+} (1.23 Å) < Nd^{3+} ($\sim$ 1.27 Å) < Sr^{2+} (1.36 Å) $\simeq$ La^{3+} ($\sim$ 1.36), as shown in the corresponding column. These last two observations imply that the values of E (%) are normalized with respect to the size of the A cation, validating the comparison of elongation percentage values obtained for the different compounds.

In $Ca_4Mn_4O_{10}$ the Ca^{2+} cations in the channels are unexpectedly more separated from each other (15.5%) than Sr^{2+} in the similar compound $Sr_4Mn_4O_{10}$ (13.2%). This is a consequence of the smaller ionic radii of Ca^{2+} that moves closer to the end of the channels to reduce Ca—O bond distances. The effect of a reduced A cation size on the perovskite network (with or without oxygen vacancies) is also visible in $CaMnO_3$ (Poeppelmeier *et al.*, 1982), where rotation of the $Mn^{4+}O_6$ octahedra along the three cubic axes is observed, yielding an orthorhombic *Pnma* structure. This rotation is thought to be caused by stabilization produced by the reduction of some and elongation of other Ca—O bond lengths, in order to satisfy the bond-valence sum rule while fitting small Ca^{2+} ions into a large cavity defined by the Mn—O network. The vacancy-ordering arrangement in $Ca_4Mn_4O_{10}$ fits smaller Ca^{2+} cations without the need for additional polyhedral tilting. The lack of observation of compounds in the $CaMnO_x$ system in bulk samples (other than the two limits $x = 2.5$ and $x = 3$) may be related to this size effect. The coexistence of 10- and 12-coordinated Ca^{2+} sites with associated local cation displacement or rotation of surrounding polyhedra, respectively, to fit Ca^{2+} bonding requirements may produce lattice distortions which are incompatible with a long-range atomic ordering. This should prevent the observation of a unique structure using bulk structural probes such as neutron or X-ray diffraction, allowing only the observation of short-range ordering through electron diffraction experiments. The effect of polyhedral rotation was mentioned by Reller *et al.* (1983) as a possible reason for having unit cells with a doubled c axis in electron-diffraction patterns for $CaMnO_{2.667}$ ($Ca_6Mn_6O_{16}$) and $CaMnO_{2.75}$ ($Ca_8Mn_8O_{22}$) compounds with respect to $Ca_4Mn_4O_{10}$. It is also possible that the smaller size of Ca^{2+} with respect to Sr^{2+} stabilizes the structural patterns with a combination of polyhedral rotations (doubling of c axis) and vacancy arrangements such as that observed for poppop ($n = 2$) and pooppoop ($n = 4$) that are related to pppp ($n = 0$), as described in §§3.1 and 3.2. This combination of factors is,

however, not enough to stabilize unique vacancy-ordering patterns for $Ca_6Mn_6O_{16}$ and $Ca_8Mn_8O_{22}$ compounds to allow their observation in bulk samples.

The different size of Nd^{3+}/La^{3+} and Sr^{2+} does not seem to promote differences among compounds which could not be explained by only considering the difference in formal charge of the cations. The charge-related distortions will now be discussed.

5.2. Charge effect

The distortions caused by the increased $A-A$ separation in the channels was mentioned in §2 as one stabilizing factor for $Sr_5Mn_5O_{13}$ and $Sr_7Mn_7O_{19}$ when combined with the apical elongation of Mn^{3+} pyramids. The main difference among Sr/$CaMnO_x$ and La/$NdCuO_x$ systems is the larger charge of the A-site cation that produces larger relative intra-channel $A-A$ elongation for the cuprates. E (%) for A^{2+} cations varies between 9 and 15.5%, and 16.5 and 22.5% for A^{3+} cations. The larger intra-channel distortion could be invoked to justify the monoclinic symmetry of both $n = 5$ $La_5Cu_5O_{13}$ and $Nd_5Cu_5O_{13}$ compounds. The large $A-A$ separation imposes a large distortion of the polyhedral network that is relieved by lowering the symmetry from tetragonal $P4/m$ to monoclinic $P2/m$, thus allowing extra structural degrees of freedom. Additionally, the acceptance of non-stoichiometric oxygen in the vacant sites, reported for $La_5Cu_5O_{13}$ and $Nd_5Cu_5O_{13}$, but not for $Sr_5Mn_5O_{13}$, is also a consequence of the larger charge and distortion imposed by A^{3+} cations in the cuprates. The inclusion of disordered non-stoichiometric oxygen reduces the average $A-A$ distance in the channels by shielding the charges.

The increase in the number of octahedra produced by a reduction in the number of oxygen vacancies imposes more rigidity on the polyhedral network, thus requiring smaller intra-channel distortions. This is clearly visible for the $n = 0$, 1 and 3 compounds in the $Sr_{n+4}Mn_4^{3+}Mn_n^{4+}O_{10+3n}$ series where E (%) decreases with increasing n. This additional rigidity of the network for larger n values could also explain the lack of observation of vacancy-ordered compounds with $n > 1$ in the $A_{n+4}Cu_4^{2+}Cu_n^{3+}O_{10+3n}$ system, owing to the impossibility of the polyhedral network to accommodate larger distortions around vacant sites. In both $LaCuO_x$ and $NdCuO_x$ systems the addition of nonstoichiometric oxygen continues in the $n = 1$ structure without other ordered phases being observed until a vacancy-disordered phase is formed for $x > 2.8$ (La Placa *et al.*, 1995; Chen *et al.*, 1995). Therefore, extra stable members of this sub-group of the $A_{n+4}B_{n+4}O_{10+3n}$ homologous series are not expected to be found.

6. Conclusions

A new homologous series of oxygen-deficient strontium manganites with perovskite structure and the general formula $Sr_{4+n}Mn_4^{3+}Mn_n^{4+}O_{10+3n}$ has been described. Compounds in the series show charge separation of Mn^{3+} and Mn^{4+} cations in pyramids and octahedra, respectively, and orbital ordering for Mn^{3+} cations. The geometrical relations among channels formed around vacant sites allow the definition of groups of polyhedra that can be used as building blocks of the series. These blocks used to generate observed and predict unobserved compounds follow the rules:

(i) building blocks consist of four $Mn^{3+}O_5$ pyramids pointing along $+x$, $-y$, $+y$, $-x$ (in this order) and n $Mn^{4+}O_6$ octahedra;

(ii) building blocks show $2/m$ symmetry;

(iii) the translation of the building block along the three lattice vectors (or linear combinations of them) generates a unique three-dimensional structural arrangement.

Generalization of the building rules to other systems has allowed us to establish a firm link among previously studied vacancy-ordering patterns of $Ca_2Mn_2O_5$, $Sr_2Mn_2O_5$, $La_2Cu_2O_5$, $La_5Cu_5O_{13}$ and $BaLa_4Cu_5O_{13}$, and the recently observed $Sr_{4+n}Mn_{4+n}O_{10+3n}$ ($n = 1$ and 3) compounds. Apical elongation of pyramidally coordinated d^4 Mn^{3+} and d^9 Cu^{2+} cations, as well as the effect of the A-site cation size and charge have been invoked to provide a qualitative explanation for the lack of observation of some members of the series for the various A and B cations.

This work has been inspired by James D. Jorgensen (1948–2006), who showed great interest and encouraged us to complete it during its early stages. We wish to thank O. Chmaissem and M. Gateshki for helpful discussion. Work at NIU was supported by the NSF Grant No. DMR-0706610 and the US Department of Transportation. At Argonne, this work was supported by the US Department of Energy, Office of Science, under contract No. DE-AC02-06CH11357.

References

Abbatista, F. & Borlera, M. L. (1981). *Ceram. Int.* **7**, 137.
Aleksandrov, K. S. & Beznosikov, V. V. (1997). *Phys. Solid State*, **39**, 695–715.
Anderson, M. T., Vaughey, J. T. & Poeppelmeier, K. R. (1993). *Chem. Mater.* **5**, 151–165.
Bednorz, J. G. & Müller, K. A. (1986). *Z. Phys. B*, **64**, 189–193.
Borlera, M. L. & Abbatista, F. (1983). *J. Less Common Met.* **92**, 55–65.
Bringley, J. F., Scott, B. A., La Placa, S. J., Boehme, R. F., Shaw, T. M., McElfresh, M. M., Trail, S. S. & Cox, D. E. (1990). *Nature (London)*, **374**, 263–265.
Caignaert, V. (1997). *J. Magn. Magn. Mater.* **166**, 117–123.
Caignaert, V., Nguyen, N., Hervieu, M. & Raveau, B. (1985). *Mater. Res. Bull.* **20**, 479–484.
Casey, P. S., Barker, D. & Hayward, M. A. (2006). *J. Solid State Chem.* **179**, 1375–1382.
Chen, B.-H., Walker, D., Scott, B. A. & Mitzi, D. B. (1996). *J. Solid State Chem.* **121**, 498–501.
Chen, B.-H., Walker, D., Suard, E., Scott, B. A., Mercey, B., Hervieu, M. & Raveau, B. (1995). *Inorg. Chem.* **34**, 2077–2083.
Chiang, C. C. K. & Poeppelmeier, K. R. (1991). *Mater. Lett.* **12**, 102–108.
Gallagher, P. K., MacChesney, J. B. & Buchanan, D. N. E. (1964). *J. Chem. Phys.* **41**, 2429–2434.
Hadermann, J., Van Tendeloo, G. & Abakumov, A. M. (2005). *Acta Cryst.* A**61**, 77–92.
Hayward, M. A. (2004). *Chem. Commun.* pp. 170–171.

Hayward, M. A., Green, M. A., Rosseinsky, M. J. & Sloan, J. (1999). *J. Am. Chem. Soc.* **121**, 8843–8854.
Hiroi, Z. (1996). *J. Solid State Chem.* **123**, 223–235.
Hodges, J. P., Short, S., Jorgensen, J. D., Xiong, X., Dabrowski, B., Mini, S. M. & Kimball, C. W. (2000). *J. Solid State Chem.* **151**, 190–209.
Jorgensen, J. D., Schuttler, H.-B., Hinks, D. G., Capone II, D. W., Zhang, K., Brodsky, M. B. & Scalapino, D. J. (1987). *Phys. Rev. Lett.* **58**, 1024–1027.
Jorgensen, J. D., Veal, B. W., Paulikas, A. P., Nowicki, L. J., Crabtree, G. W., Claus, H. & Kwok, W. K. (1990). *Phys Rev. B*, **41**, 1863–1877.
Khasanova, N. R., Izumi, F., Hiroi, Z., Takano, M., Huang, Q. & Santoro, A. (1996). *Acta Cryst.* C**52**, 2381–2384.
La Placa, S. J., Bringley, J. F., Scott, B. A. & Cox, D. E. (1993). *Acta Cryst.* C**49**, 1415–1417.
La Placa, S. J., Bringley, J. F., Scott, B. A. & Cox, D. E. (1995). *J. Solid State Chem.* **118**, 170–175.
Michel, C., Er-Rakho, L. & Raveau, B. (1985). *Mater. Res. Bull.* **20**, 667–671.
Mitchell, R. H. (2002). *Perovskites: Modern and Ancient.* Ontario: Almaz Press Inc.
Moriga, T., Hayashi, M., Sakamoto, T., Orihara, M. & Nakabayashi, I. (2002). *Solid State Ion.* **154**, 251–255.
O'Malley, M., Lockett, M. A. & Hayward, M. A. (2007). *J. Solid State Chem.* **180**, 2851–2858.
Poeppelmeier, K. R., Leonowicz, M. E., Scanlon, J. C., Longo, J. M. & Yelon, W. B. (1982). *J. Solid State Chem.* **45**, 71–79.
Reller, A., Jefferson, D. A., Thomas, J. M., Beyerlein, R. A. & Poeppelmeier, K. R. (1982). *J. Chem. Soc. Chem. Commun.* pp. 1378–1380.
Reller, A., Jefferson, A., Thomas, J. M. & Uppal, M. K. (1983). *J. Phys. Chem.* **87**, 913–914.
Reller, A., Thomas, J. M., Jefferson, D. A. & Uppal, M. K. (1984). *Proc. R. Soc. London Ser. A*, **394**, 223–241.
Ruiz-González, M. L., Cortés-Gil, R., Alonso, J. M., Hernando, A., Vallet-Regí, M. & González-Calbet, J. M. (2006). *Chem. Mater.* **18**, 5756–5763.
Shaked, H., Keane, P. M., Rodriguez, J. C., Owen, F. F., Hitterman, R. L. & Jorgensen, J. D. (1994). *Crystal Structures of the High-Tc Superconducting Copper-Oxides.* Oxford: Elsevier Science, BV.
Shannon, R. D. (1976). *Acta Cryst.* A**32**, 751–767.
Suescun, L., Chmaissem, O., Mais, J., Dabrowski, B. & Jorgensen, J. D. (2007). *J. Solid State Chem.* **180**, 1698–1707.
Suescun, L., Dabrowski, B., Mais, J., Remsen, S., Richardson Jr, J. W., Maxey, E. R. & Jorgensen, J. D. (2008). *Chem. Mater.* **20**, 1636–1645.
Wu, M. K., Ashburn, J. R., Torng, C. J., Hor, P. H., Meng, R. L., Gao, L., Huang, Z. J., Wang, Y. Q. & Chu, C. W. (1987). *Phys. Rev. Lett.* **58**, 908–910.
Yamauchi, H., Karpinnen, M. & Tanaka, S. (1996). *Phys. C*, **263**, 146–150.